*Manuscript
Click here to view linked References

Improved antitumor effect of paclitaxel administered *in vivo* as pH and glutathione-sensitive nanohydrogels

Elena Pérez[1], Ana Martínez[2], César Teijón[3], Rosa Olmo[4], José María Teijón[5], María Dolores Blanco [*]

1. Dpto. Bioquímica y Biología Molecular III. Facultad de Medicina. Ciudad Universitaria s/n, UCM. 28040 Madrid. E-mail: elenpe01@ucm.es

2. Facultad de Farmacia. Universidad Francisco de Vitoria. Madrid (Spain). E-mail: am.martinez.prof@ufv.es

3. Dpto. Enfermería. Facultad de Enfermería, Fisioterapia y Podología. Ciudad Universitaria s/n, UCM. 28040 Madrid E-mail: cteijon@enf.ucm.es

4. Dpto. Bioquímica y Biología Molecular III. Facultad de Medicina. Ciudad Universitaria s/n, UCM. 28040 Madrid. E-mail: rmolmo@med.ucm.es

5 Dpto. Bioquímica y Biología Molecular III. Facultad de Medicina. Ciudad Universitaria s/n, UCM. 28040 Madrid. E-mail: jmt@med.ucm.es

*Corresponding author. Dpto. Bioquímica y Biología Molecular III. Facultad de Medicina. Ciudad Universitaria s/n, UCM. 28040 Madrid.Telephone: + 34 91 394 1447; Fax number: +34 91 394 1691; E-mail: mdblanco@med.ucm.es

Abstract

Most antitumor drugs usually affect not only rapidly dividing cells, such as those in tumors, but also highly proliferative cells in normal tissues. This nonspecific drawback could be successfully solved by using nanocarriers as controlled drug delivery systems. In this work, pH and redox-responsive nanohydrogels (NG)

based on N-isopropylacrilamide (NIPA), N-hydroxyethyl acrylamide (HEEA) 2-acrylamidoethyl carbamate (2AAECM) and N´-N´cystaminebisacrylamide (CBA) as crosslinker were evaluated as bioreducible paclitaxel (PTX) nanocarriers for improving the accumulation of the drug within the tumor tissue and avoiding its conventional side effects. A single dose of PTX solution, unloaded-NHA 80/15/5CBA NG and PTX-loaded NHA 80/15/5-CBA NG (30mg/kg PTX equivalent) were subcutaneously injected in female athymic nude mice bearing HeLa human tumor xenografts. PTX-loaded nanohydrogels showed higher antitumor activity than free PTX, as tumor evolution and Ki67 detection demonstrated. Histological tumor images revealed a higher content of defective mitotic figures and apoptotic bodies in PTX- treated tumors than in control or unloaded NG treated tumor samples. Nanohydrogels injection did not change any biochemical blood parameters, which means no liver or kidney damage after NG injection.However, differences in antioxidant defenses in MPS systems (liver, kidney and spleen) were observed among treatments, which may indicate an oxidative stress response after PTX injection.

Keywords: anti-tumor efficacy, *in vivo* toxicity, paclitaxel, stimuli responsive nanohydrogel, histopathology, oxidative stress

1. Introduction

Cancer is the leading cause of death in economically developed countries and the second leading cause of death in developing countries. The global impact of cancer continues to increase largely because of the aging and growth of the world population alongside an increasing adoption of cancer-causing behaviors, particularly smoking, in economically developing countries (Jemal et al., 2011). In the last decades, nanotechnology has emerged to improve the therapeutic index of existing chemotherapies and radiotherapy treatments which, in combination with cancer biology advances, can establish new methods for cancer care (Hull et al., 2014).

Most antitumor drugs affect not only rapidly dividing cells, such as those in tumors, but also highly proliferative cells in normal tissues. This nonspecific drawback has limited the clinical application of most anticancer drugs (Li et al., 2009). For instance, paclitaxel (PTX) exhibits a significant activity against various solid tumors, including advanced ovarian carcinoma, metastatic breast cancer, non-small cell lung cancer, and head and neck carcinomas (Panchagnula, 1998; Spencer and Faulds, 1994). It interferes with mitosis by binding to the β-subunit of tubulin and forming stable, non-functional microtubule bundles, causing cell death by disrupting the dynamics necessary for cell division (Crown and O'Leary, 2000). However, its formulation with Cremophor® EL and ethanol, due to its high hydrophobicity, supposes several side effects such as hypersensitivity reactions, nephrotoxicity and neurotoxicity (Singla et al., 2002). Thus, to achieve the necessary therapeutic effect of PTX in

the desired tumor tissue, suitable carriers for PTX are needed. Many vehicles have been proposed as good candidates for use as controlled delivery systems (Yared and Tkaczuk, 2012), but few have progressed to *in vivo* or clinical studies.

To reach the goal, stimuli-sensitive polymers have been recently studied for drug delivery (Fleige et al., 2012; Lee et al., 2008), as they can modify their structural composition/conformation specific cellular/extracellular in response to chemical, biochemical, or physical stimulus, promoting release of the active species to specific biological environment (Motornov et al., 2010). For instance, the high glycolysis showed in solid tumors supposes acidic pH, which can be as low as 5.7, depending on tumor histology, tumor volume and the location within a tumor (Engin et al., 1995; Tannock and Rotin, 1989). pH gradient also affects the ionization, intratumoral distribution and cellular uptake of ionizable drugs in a tumor (Gao et al., 2005). Thus, a variety of polymeric pH-sensitive components with cleavable bonds have been described, which contain reversible ionizable groups, such as carboxylic or amino groups, such as *N´*-hydroxyethyl acrylamide (HEAA), which allow the swelling of nanogels by electrostatic repulsion (Blanco et al., 2002; Qiao et al., 2011). Otherwise, it is also well known that tumor tissues are highly reducing and hypoxic compared with normal tissues, which means an increase of 7–10 fold higher content of intracellular glutathione (GSH) in tumor cells than in normal cells (Kuppusamy et al., 1998). This combination of intracellular elevated GSH and the tumor associated GSH make redox-responsive nanocarriers interesting candidates for targeted drug release. These reduction-sensitive polymers and conjugates

show an excellent stability in the circulation and in the extracellular fluids, whereas they are prone to rapid disintegration under a reductive environment present in intracellular compartments, such as the cytoplasm and the cell nucleus (Meng et al., 2009). For this reason, drug delivery systems containing disulfide linkages such as N, N'-cystaminebisacrylamide (CBA) provide significant improvements to cytosolic and nucleus drug targeting, where disulfide linkages are rapidly degraded by GSH (Song et al., 2011). Thus, in the last decades many engineered nanocarriers have been designed based on these polymers (Fleige et al., 2012; Klinger and Landfester, 2012; Motornov et al., 2010). Moreover, nanohydrogels resemble natural living tissue more than any other class of synthetic biomaterials (Peppas et al., 2000). Their low interfacial tension reduces their tendency to adsorb proteins from body fluids and their three-dimensional structure facilitates a faster diffusion into (drug loading) and out of (drug release) hydrogels to different molecule sizes, which allows the possible use of these polymeric networks as drug delivery systems (Gupta et al., 2002).

In our previous work, new stimuli-responsive nanohydrogels based on poly-N-isopropylacrilamide (NIPA),N-hydroxyethyl acrylamide (HEAA) and tert-butyl 2-acrylamidoethyl carbamate (2AAECM) were synthesized by a microemulsion polymerization method using N,N-cystaminebisacrylamide (CBA) as a crosslinking agent, to obtain bioreducible drug carriers for PTX encapsulation (Perez et al., 2014). Cell culture studies revealed effective and cytocompatible nanocarriers for hydrophobic anticancer drugs delivery, such as paclitaxel. Thus, in this study, the *in vivo* anti-tumor effect of those PTX-loaded nanohydrogels was investigated by using female athymic nude mice bearing

HeLa human tumor xenografts to insure maximal therapeutic efficacy with minimal side effects, increasing drug residence at the target site and improving cellular uptake and intracellular stability.

2. Materials and methods

2.1. Materials

Sodium hydroxide (NaOH), hydrochloric acid (HCl; 37%), sodium chloride (NaCl), ethanol absolute, xylene, Triton X-100, phosphoric acid (85% w/ v) anhydrous di-sodium hydrogen phosphate (Na_2HPO_4) and di-hydrogen potassium phosphate (KH_2PO_4) were purchased from Panreac (Barcelona, Spain). Bovine serum albumin (BSA, Fraction V) and disodium hydrogen phosphate dehydrated were purchased from Merck (Barcelona, Spain).Paclitaxel (Taxol) was supplied by Tocris Bioscience (Mw 889.95 > 99%). Paraformaldehyde, Commasie-blue G-250 and gentamicin were purchased from Sigma–Aldrich (Barcelona, Spain). Dulbecco's modified Eagle medium + GlutaMax (DMEM) was purchased from Lonza (Belgium). 0.05% trypsin/0.53 mM EDTA, penicillin and streptomycin were purchased from Invitrogen Life Technologies (Grand Island, NY). Hydrogen peroxide solution was obtained from Fluka. All water used in the biochemistry analysis was Millipore Milli Q grade. All the chemicals used were of the highest commercially quality available

2.2. Preparation and characterization of nanohydrogels

Copolymeric nanohydrogels of N-isopropylacrylamide (NIPA), N-hydroxyethyl acrylamide (HEAA) and 2-acrylamidoethyl carbamate (2AAECM) (Agüero et al., 2010) using N-N´-cystaminebisacrylamide (CBA) as the crosslinking agent were obtained by microemulsion polymerization, as described before (Perez et al., 2014). In the present study, we evaluate the nanohydrogel formulation composed by NIPA/HEAA/2AAECM-CBA 80:15:5:5 namely as NHA 80/15/5-CBA.

After the purification process, paclitaxel (PTX) was encapsulated by immersion of 50 mg of the nanogel in a PTX/ethanol solution (10 mg/mL) at room temperature (22°C) in the dark for 24 h. The suspension was then centrifuged at 7,000 rpm for 5 min (Digicen20-R Ortoalresa Centrifuge, Radius 8.2 cm rotor; Madrid, Spain) and the pellet dried (Bioblock Scientific 45001, France) until the ethanol had completely evaporated. The amount of PTX loaded in the nanosystems was determined by high-performance liquid chromatography (HPLC) as described in our previous work (Perez et al., 2014). All quantifications were performed in triplicate and drug encapsulation efficiency (%) was calculated as previously described (Perez et al., 2014).

Zeta potential of unloaded- and PTX-loaded nanohydrogels was analyzed from a dispersion of those nanosystems in distilled water (Zeta Potential Analyzer, Brookhaven, Ins.Corp.).

2.3. In vivo antitumor efficacy studies

- **Cell culture.** Human cervical cancer cells (HeLa) were cultured and maintained in DMEM+GlutaMax-I supplemented with 10% heat inactivated

fetal bovine serum, penicillin (50 U/mL), streptomycin (50 µg/mL) (Invitrogen Life Technologies, Grand Island, NY, USA) and gentamicin (50 µg/mL) (Sigma–Aldrich Company, United Kingdom) in a humidified incubator at 37°C and 5% CO_2 atmosphere (HERA cell, Sorval Heraeus, Kendro Laboratory Products GmbH, Hanau, Germany). Cells were plated in 75 cm^2 flask (Sarstedt Ag and Co., Barcelona, Spain) and were passaged when reaching 95% confluence by gentle trypsinization (0.05% trypsin/0.53 mM EDTA; Invitrogen Life Technologies). The cells were harvested during the logarithmic growth phase and re-suspended in serum free medium before inoculation in animals.

- **Experimental model.** The experimental protocol involving use of animals was approved by the Institutional Animal Care and Use Committee of Complutense University of Madrid. Female athymic mice (Nu/Nu strain), 4–6 weeks old, weighing 20 ± 3g were purchased from Harlan Laboratories (Indianapolis, USA) and were housed under controlled laboratory conditions in polycarbonate cages having free access to sterilized rodent pellet diet and water *ad libitum*. The animals were allowed to acclimate for at least 48 hours before any experiments.

- **Subcutaneous tumor xenograft development.** 9 x 10^6 HeLa cells, suspended in 200 µl of serum free medium were injected subcutaneously into the dorsal side of mice under light isoflurane anesthesia. Palpable solid tumors developed within 14-16 days post tumor cell inoculation and as soon as tumor volume reached ~140 mm^3, the animals were randomly allotted to four different groups (6 animals per group): control (saline serum), free PTX in

aqueous solution, unloaded-NHA 80/15/5-CBA NG and PTX-loaded NHA 80/15/5-CBA NG

- ***In vivo* administration of the formulations.** Six lightly-anesthetized animals per group were used for the experiments. Each lightly-anesthetized tumor-bearing animal received PTX at a single dose of 30 mg/ kg either in aqueous solution or in PTX-loaded NHA 80/15/5-CBA nanohydrogels (30mg/kg of PTX equivalent) by subcutaneous administration (200 µL) in the surroundings of tumor.
- **Evaluation of therapeutic efficacy.** Animal weight was recorded three times a week. The tumor diameters were also measured three times weekly with vernier calipers in 2 dimensions. Individual tumor volumes (V) were calculated using the formula: $V = [\text{length} \times (\text{width})^2]/2$ where length (L) is the longest diameter and width (W) is the shortest diameter perpendicular to length. Moreover, tumor volume evolution was divided into two different stages f(rom day 14 to day 30; and from day 30 to day 39) in order to calculate tumor growth rate in those periods of time (V2: 14-30, V3: 30-39). The tumor growth ratio for each phase was calculated using the tumor growth rate established in the first phase, before treatments (V1; V1 = 12.9 mm3/day (r2= 0.97)) (Table 1). Following the completion of treatment schedule, mice were sacrificed and tumors were isolated, weighted and post-fixed in paraformaldehyde 4% for histopathological and immunohistochemical analysis. Plasma samples, liver, kidney, spleen, lung, heart, ovary and uterus were also collected, weighted and frozen for later characterization studies.

2.4. Tumor histology and Immunohistochemistry Studies

After the post-fixation step, tumors were washed by successive dipping in ethanol and xilene, and embedded in Paraplast® (Surgipath®, Leica). For histological observations, the tumors were cut into 8 µm sized sections using a microtome blade, fixed on the glass slide for overnight at 37 °C, and mounted using glass coverslip for observation under a microscope. The tumor sections were analyzed for histology by optical microscopy using the alcian blue hemalum picro-indigo, the toluidine blue, and the hematoxylin–eosin methods (Humason, 1979). 5 µm sized tumor sections were cut in order to develop immunohistochemical studies. These studies were carried out using the Ki-67 labeling test (Patel and Amiji, 1996). Ki-67, a nuclear antigen expressed in proliferating cells and absent in resting cells, was qualitatively determined incubating the samples with purified mouse anti-human Ki-67 antibody (1:25, BD Biosciences Pharmingen, USA) and revealed them after by a fluorescence method. After the incubation with the mouse antihuman Ki-67 antibody, samples were incubated with a rabbit antimouse-rhodamine as second antibody (1:100, BD Biosciences Pharmingen), then washed and mounted with Dapi-Fluoromount-G (SouthernBiotech, AL, USA) for observation by light fluorescence microscopy. To ensure specific staining of the Ki-67 positive cells, some tissue sections were treated only with the second antibody.

2.5. Blood biochemistry analysis and Oxidative Stress

Once collected blood in heparin tubes, plasma was obtained by centrifugation (3500rpm; 15min; 4ºC) to determine several parameters related to liver:

aspartate aminotransferase (AST), alanine aminotransferase (ALT) and alkaline phosphatase (ALP); and kidney functions: blood urea nitrogen (BUN) and creatinine (CRE). Assays were performed by enzyme assay kits (Biosystems®, Spain) and data were obtained using a spectrophotometer (Evolution 201, Thermo Scientific, Spain).

Otherwise, once organ samples were extracted, they were frozen (-80ºC) for later enzymatic activity analysis, in order to evaluate antioxidant defenses. For this purpose, tissue samples from liver, kidney and spleen were weighted and homogenized (Heidoloph RZR 2050 electronic) at 1200 rpm in ice-cold NaCl 0.9% (w/v) and 10µL heparin. The homogenates were mixed with four volumes of Triton X-100 (1%, v/v) and the residual fragments were removed by centrifugation at 12,500 rpm for 15 min. Later, total antioxidant capacity (TAC; Oxiselect™, Cell Biolabs, Inc.), superoxide dismutase activity (SOD; Oxiselect™, Cell Biolabs, Inc.), total glutathione (Oxiselect™, Cell Biolabs, Inc.) and glutathione reductase activity (Abnova, UK) were performed by enzyme assay kits. Catalase activity was determined by following Aebi method (Aebi, 1984): 60µL serum was mixed with 1mL of peroxide hydrogen 3% (w/v) diluted in phosphate buffer (50Mm, pH 7). Finally, total protein was assayed by Bradford method (Bradford, 1976).

2.6. Statistical data analysis

Results were expressed as a mean ± standard deviation (SD). Statistical analysis was performed using one way analysis of variance (ANOVA) following by Bonferroni *post hoc* analysis with computer software SPSS 22.0.

A p-value < 0.05 and p < 0.01 were considered significant and very significant, respectively

3. Results

3.1. Preparation and characterization of nanohydrogels

Nanohydrogel drug content studies showed a loading capacity of 47.4 ± 5.4 µg PTX/mg NG, and an encapsulation efficiency of 48.5%. Besides, zeta potential evaluation revealed anionic surface in both unloaded and drug loaded nanohydrogels (-2.75 mV in unloaded NHA 80/15/5-CBA NG and -18.11 mV in PTX-loaded NHA 80/15/5-CBA NG).

3.2. *In vivo* antitumor efficacy studies

In order to evaluate the safety of the treatments, body weight was monitored during the period of experiment. Results showed that body weight of all animals increased normally with age (Fig. 1), with no differences among groups. Moreover, no significant changes were found in organosomatic index in any of the animal groups (Fig. 2).

Tumor volume was measured every two days until day 39 in order to evaluate the tumor evolution (Fig.3). Neither toxicity-induced death nor complete tumor growth regression was observed in any experimental group.

As shown in Fig.3, tumor volume increased rapidly when the mice were treated with saline serum or unloaded NHA 80/15/5-CBA nanohydrogels. Little differences were found between the tumor evolution of these two groups. Tumor growth rate (Table 1) showed two different growth kinetic phases, with a good

correlation value (r^2). During the first stage (14-30 days), a slower tumor growth rate was observed (21.9-42.6 mm^3/day for control and unloaded-NG groups, respectively), with a tumor growth ratio of 1.7-3.3 respectively. During the second stage (30-39 days), a rapid tumor growth of 94.5-58.5 mm^3/day was seen, which corresponds to 7.3-4.5 tumor growth ratios. In the case of tumors treated with PTX (free PTX and PTX-loaded nanohydrogels) significant differences ($p<0.01$) were obtained when compared with control saline group (Fig.3). Additionally, the antitumor activity of PTX-loaded nanohydrogel treatment was higher than the observed in free PTX treated mice (Fig.3), which was in accordance to tumor growth rate and ratio. As observed in Table 1, tumor growth rate showed two different stages, with a good correlation value (r^2), where free PTX group demonstrated a more rapid tumor growth (33.0 mm^3/day at the first stage and 36.9 mm^3/day at the second stage) than in PTX-loaded NG group (20.6 mm^3/day at the first stage and 8.01 mm^3/day at the second stage). Moreover, tumor growth at the second stage was the slowest growth rate during the whole experiment, with a tumor growth ratio of 0.6.

3.3. Tumor histology and Immunohistochemistry Studies

To further evidence the observed anticancer activity, the tumor tissues of mice either untreated or treated were subjected to histological observation, employing the hematoxylin-eosin (Fig. 4), the toluidine blue and the alcian blue hemalum picroindigo (trichromic) methods (Fig. A.1)

As it can be observed in Fig. 4, the epithelial-like cortex of the untreated and unloaded nanohydrogels-treated tumors (Fig. 4 a-d) was composed of poorly cohesive heterogeneous cells, mostly polyhedral in shape, with a large nucleus/cytoplasm index. In these images, some nucleus revealed a dispersed chromatin and prominent nucleoli, although mitosis was also observed. Moreover, images showed a low presence of connective tissue and some necrosis areas. An extensive lymphocyte infiltration into tumor tissue was also shown.

Otherwise, differences in tumor histology could be observed in the tumor cells of the epithelial-like cortex of PTX-loaded nanohydrogels treated mice, as well as free PTX treated animals. First, Figs. 4e-h images showed an increase in the amount of defective mitotic figures, observed as hyperchromatic objects (yellow circles) and several apoptotic bodies (black square), and necrosis areas (red arrow). In addition, the tissue seems to be more retracted and higher disorganized than untreated tumors (Fig. 4e and g).

Additionally, in order to differentiate proliferating cells remaining in the tumor tissue from dead cell populations, Ki-67 cell proliferation assay was carried out by immunohistochemical staining of the tumor sections (Fig.5).Thus, the presence of the antigen was visualized using a fluorescence dye (fluorescence microscopy). As it is shown in Fig. 5E and F, the highest fluorescent signals of Ki67 antigen were obtained from tumors treated with free paclitaxel, which was similar to that obtained in untreated and unloaded treated tumors (Fig. A.2). In contrast, very low fluorescent signal was observed in case of PTX-loaded

342 nanohydrogel samples (Fig.5 B and C). This result means a lower presence of
343 the antigen in these tissues, even in the blood vessel surrounding area, and
344 therefore an enhanced antitumor activity efficacy of the drug.
345
346 **3.4. Blood biochemistry analysis and Oxidative Stress**

347 Potential pathological lesions in liver and kidney induced by the administration
348 of nanohydrogels can be characterized by an increase in biochemical
349 parameters including the liver and the kidney function markers. Thus, various
350 biochemical serum parameters were tested from both treated and untreated
351 animals. As shown in Table 2, no significant differences ($p < 0.05$) were obtained
352 among control group and nanohydrogel treatments in AST, ALP, BUN and CRE
353 levels. Nevertheless, a significant increase ($p < 0.05$) of ALT activity was
354 observed in free-PTX treated animals, when compared with control group and
355 PTX-NHA 80/15/5-CBA treatment. Furthermore, a significant decrease ($p
356 < 0.05$) in creatinine levels was observed in free PTX treated mice, when
357 compared with control group and PTX-NHA 80/15/5-CBA treatment.

358 Otherwise, oxidative stress is proposed as one of the most important
359 mechanisms for nanotoxicity. Thus, to evaluate a possible association among
360 oxidative response with nanohydrogels injection, different antioxidative
361 parameters were evaluated in liver, kidney and spleen (Fig.6). Results obtained
362 from antioxidant defenses analysis in the liver revealed a significant decrease
363 ($p < 0.05$) in superoxide dismutase (SOD) and catalase activities (CAT) in PTX
364 solution and PTX-NHA 80/15/5-CBA treatment groups. In the case of kidney,
365 assays revealed similar results between all treatments in SOD and CAT

activities. However, a significant increase ($p < 0.05$) in GSSG-R activity was observed in spleen samples extracted from PTX-loaded NG mice, comparing with control group. Moreover, a significant increase in total glutathione content (GSSG/GSH) was also observed in free PTX and PTX-loaded NG groups at kidney samples.

4. Discussion

Controlled drug delivery systems release bioactive agents at predetermined rates for predefined periods of time and have been used to overcome the shortcomings of conventional drug formulations (Qiu and Park, 2012). As observed in our previous *in vitro* work (Perez et al., 2014), NHA 80/15/5-CBA nanohydrogels may be used as potential carriers for PTX delivery in order to increase its solubility and reach a pharmacological concentration, avoiding the side effects of the conventional formulation (Reul et al., 2011). *In vitro* characterization showed nanoscale spherical hydrogels (in the size range of 10-80 nm at physiological conditions). *In vitro* drug release studies revealed an incomplete PTX release from those nanohydrogels along the first 50 hours, with a maximum PTX release of 58.8% (19.74 ± 2.39 µg/mg NG). Two different stages were observed during this period: a rapid drug release within the first 5h and a more controlled drug release in the last 45h of the experiment. In this previous work (Perez et al., 2014), a tight dependence between the amounts of the drug released from particles and the pH and GSH medium levels was observed. In a release medium without GSH, results showed a more rapid drug release at pH 5 (1.39 µg PTX/h) due to electrostatic repulsion between a protonated amino group of HEAA monomer, resulting in nanohydrogel swelling

and, therefore, a faster drug release. Nevertheless, the most rapid PTX release was obtained in an intracellular GSH concentration medium (K value between 1.86 µg PTX/h −2.15 µg PTX/h). These data revealed that this accelerated PTX release from nanohydrogels might be due to the reduction of crosslinking agent (CBA) disulfide linkages by GSH content. Here, we evaluate the safety and the effectiveness of those nanosystems *in vivo* in a xenograft tumor model. Results indicated there were no significant differences in body weight changes among the experimental groups during the experimental time period (Fig.1). The mice receiving PTX-loaded NHA 80/15/5-CBA nanohydrogels showed similar body weight curves to the saline-treated mice, which implied that NHA 80/15/5-CBA nanohydrogels did not have severe toxicity in regards to body weight changes. Besides, organosomatic index results (Fig.2) also demonstrated no significant differences among treatments, which may be interpreted according to the safety and effectiveness of these nanosystems in the tumor treatment. Moreover, those results were also in accordance to zeta potential analysis results, which revealed a negative surface charge. As several authors demonstrated (Mayer et al., 2009; Sharifi et al., 2012), anionic surface seems to be less hematotoxic than cationic surface particles, as positively charged particles showed higher affinity to the negative phospholipid head groups or protein domains on cell membranes (Goodman et al., 2004).

In order to confirm the anti-tumor effect of PTX-loaded nanohydrogels, the mice were treated with nanohydrogels and free PTX at a single dose of 30mg/kg. As expected, no significant tumor regression was observed in the placebo-treated group confirming that unloaded NHA 80/15/5-CBA nanohydrogels do not have

anti-tumor activity (Fig.3). Moreover, tumor growth rates and tumor growth ratio of unloaded nanohydrogels group demonstrated a rapid evolution of the tumor at the final stage, which was similar to control saline group (Table 1). In our study, tumor growth rates and ratios were lower in PTX-loaded nanohydrogel group than in free PTX group during the whole experiment (Table 1). When PTX was freely administered in solution, tumor seemed to stop growing during the first stage (14-30 days), as observed when tumor growth rate (33.0 mm^3/day) was compared with tumor growth rate of unloaded-NG group (42.6 mm^3/day); however, the antitumor activity of free-PTX was not effective enough to cause the stabilization of tumor growth. After the day 30, tumors treated with free PTX recovered its capacity of proliferation, reaching a tumor growth rate (36.9mm^3/day) similar to those obtained at the first stage in control and unloaded-NHA 80/15/5-CBA NG groups. In addition, tumor growth suppression was observed in PTX-loaded nanohydrogel group (Fig.3; Table 1) in the last nine days of the experiment (from day 30 to day 39), as expected for sustained and controlled drug release in the targeted tumor sites and tumor cells. These results could be explained by the rapid degradation of free PTX within the tumor tissue site by hydrolytic process (Iqbal et al., 2011), while PTX loaded in nanosystems was protected from hydrolytic degradation, maintaining drug concentration within the therapeutic window (Zhang et al., 2013). These results were in accordance to Chun *et al.* studies (Chun et al., 2009), and demonstrated that PTX-loaded nanohydrogels require more time for cellular uptake and drug release than free PTX for effective tumor inhibition, and for minimal systemic side effects over a prolonged time period (over a month).

These *in vivo* antitumor effects confirmed that PTX-loaded nanohydrogels could improve the chemotherapeutic efficacy of free PTX, according to Shim et al. (Shim et al., 2007) study, where PTX was encapsulated in pH and temperature hydrogels and subcutaneously injected into C57BL/6 male mice at 25 and 50 mg/kg PTX dose. This improved antitumor effect may be explained by the increasing drug residence at the target site due to the high cellular uptake and intracellular stability, as demonstrated in previous studies (Perez et al., 2014). Once the drug vehicle reaches the cell, the particle is shuttled from the early endosome to the late endosome and finally the lysosome for degradation (Steichen et al., 2013). Throughout this pathway the pH decreases from 7.4 to approximately 5.0, leading to the expansion of these cationic nanogels, due to the charge repulsion between neighboring protonated amine groups of HEAA monomer as observed in our previous work (Perez et al., 2014). Consequently, a faster drug release was obtained. Additionally, contained within the intracellular components are enzymes and GSH molecules that aid in foreign body degradation (Steichen et al., 2013). Moreover, PTX was mainly released from these nanocarriers once CBA crosslinking hydrogel desintegration occurred, by disulfide linkages reduction in the presence of GSH, which means a reduction of side effects by targeting to disease site and target cells.

Otherwise, particles in the size range of 20–200nm, such as these nanohydrogels (10–80 nm in the collapsed state) (Perez et al., 2014), could easily extravasate through endothelial pores (50–100 nm in size) and accumulate inside the interstitial space for a long time, due to the inefficient lymphatic drainage observed in the solid tumors (Kwon et al., 2008; Steichen et al., 2013). This size also provides increased diffusivity, biodistribution, absence

of immunogenicity, and the ability to target specific tissues with minimal distribution to other tissues (Moghimi et al., 2001).

Histological analysis, using both routine and immunohistochemical staining methods, is a common procedure for obtaining pathological information (Fig. 4). Tumor sections from PTX-loaded nanohydrogels treated mice and free PTX treated mice showed a high density of defective mitotic cells, apoptotic bodies, as well as necrosis areas. These results were in accordance to the microtubule depolymerization process carried out by taxanes. Microtubules are heterodimeric α/β-tubulin filaments implicated in diverse cellular functions beyond cell division, such as growth, motility, the development and maintenance of cell shape, and the trafficking of vesicles, organelles, and proteins (Andreopouloua and Muggia, 2008). Paclitaxel acts to stabilise microtubules, causing the cell cycle arrest at the G2/M checkpoint of mitotically active cells (Kumar et al., 2015) as showed in our previous work (Perez et al., 2014); thereby it inhibits cell replication, which in turn results in apoptosis (Panchagnula, 1998), according with the results obtained from free PTX and PTX-loaded nanohidrogels (Fig. 4). Furthermore, recent studies from glioma stem cells after PTX treatment showed that polymorphic nuclei signs such as the presence of defective mitotic figures, uncondensed chromatin threads, chromosome fragmentation and de-condensed chromosomes were time-dependent (Riva et al., 2014).This mitotic activity is a crucial parameter to measure the aggressiveness of a tumor and it is therefore associated with important clinical implications. Thus, various biological parameters are routinely studied for their ability to predict responses to anticancer drugs, including the

nuclear protein Ki67, which has demonstrated strong prognostic effects and has been predictive of a greater response to most chemotherapies (Tozuka et al., 2013). Our results revealed a lower presence of this tumor proliferation indicator in PTX-loaded NHA 80/15/5-CBA nanohydrogel treated tumors, compared with untreated or free PTX treated tumors (Fig. 5). These results, together with tumor evolution analysis suggested that PTX-loaded NHA 80/15/5 CBA nanohydrogel was the most effective treatment. Moreover, our water-soluble PTX-nanohydrogel formulation is Cremophor-free. The same conclusions were obtained from a study by Shim *et al.* (Shim et al., 2007) where PTX-loaded block copolymer subcutaneous injectable hydrogel could effectively suppress the tumor proliferation, as revealed immunohistological apoptotic cells detection. Also, Liu *et al.* (Liu et al., 2008) showed similar results after intravenous injection of PTX-loaded carbon nanotubes (5 mg/kg) in 4T1 tumor-bearing Balb/c mice.

Most of the injected nanoparticles are taken in and eliminated by mononuclear phagocyte system (MPS), including liver and kidney tissue (Li and Huang, 2008.). Moreover, drug biodistribution results obtained from different research groups (Kim et al., 2001; Liu et al., 2008; Wang et al., 2013; Zhang et al., 2008) demonstrated PTX was mainly distributed in spleen, kidney and liver tissues and the most antitumor drugs affect not only rapidly dividing cells such as those in tumors, but also those in highly proliferative normal tissues (Lia et al., 2009).Thus, various biochemical parameters and antioxidant defenses were tested in order to analyze potential pathological lesions in those organs induced by the injection of NHA 80/15/5-CBA nanohydrogels. Results from biochemical

blood parameters (Table 2) revealed no liver or kidney damage in unloaded nanohydrogel treated mice and PTX-loaded treated nanohydrogel mice, as ALT, AST, ALP, BUN and CRE levels were similar to those obtained from control-saline group and in good agreement with the reference normal ranges for mice (Chen et al., 2003; Pagel et al., 2003; Wang et al., 2013). Similar conclusions were obtained by Wang *et al.* studies (Wang et al., 2013) where PTX loaded PEGylated poly(□-caprolactone-co-L-lactide) micelles were intravenously injected in S180 tumor-bearing mice at different PTX dosage (10, 20 and 30 mg/kg). In contrast, free PTX-treated mice showed a significant increase of alanine aminotransferase activity (ALT) and a significant decrease of creatinine blood level. These results may indicate liver and kidney damage after free PTX injection and were in accordance with Mo-ying *et al*. studies (Mo-ying et al., 2004), which revealed liver injuries in S-180 mice after PTX injection. Authors also observed that the mechanisms of the liver injuries are correlated with oxidative stress after administration of the drug.

As mentioned above, a little amount of these subcutaneously administrated nanohydrogels, as well as their residual bodies, may extravasate through endothelial pores (50–100 nm in size) and achieve MPS organs, such as liver, kidney or spleen. Therefore, in the present study, oxidative stress response was also evaluated after nanohydrogels injection (Fig. 6). Oxidative stress occurs when there is an excess of free radicals in the body, which are constantly produced in normal physiological conditions during metabolic processes in all living species (Sharifi et al., 2012). Nevertheless, an excessive reactive oxygen species (ROS) accumulation will lead to cellular injury, ending up in many physiological problems, such as ageing, asthma, arthritis, diabetes, cancer,

inflammation and cardiovascular disease (Oberdörster et al., 2005). To prevent that, tissues have developed an antioxidant defense system that includes non-enzymatic antioxidants such total glutathione content (GSSG/GSH) and enzymatic activities like SOD, CAT and GSSG-R (Simmons, 1984). Our results revealed lower activity levels of SOD and CAT in the liver of subcutaneous administered free PTX solution group and in the PTX-loaded nanohydrogels treated group, in comparison to control group, indicating higher level of oxidative stress due to PTX injection (Fig. 6). Similar results were obtained by Kalaria *et al.* (Kalaria et al., 2009), where doxorubicin solution as well as doxorubicin-loaded PLGA nanoparticles were orally and intravenously administrated in female Sprague–Dawley rats. Thus, significant changes on SOD and CAT activities in the liver of athymic mice after PTX solution and PTX-loaded nanohydrogels injection were observed. SOD scavenges $O2^{-\bullet}$ anion (which is the first product of oxygen radicals) to form H_2O_2 and, therefore, diminishes the toxic effects due to the free radicals derived from secondary reactions. Besides, the $O2^{-\bullet}$ anion inactivates CAT activity, which is a major determinant of hepatic anti-oxidant status, involved in detoxification of high H_2O_2 concentrations (Zhang and Kwong-Huat, 2000). Thus, a low SOD activity means a decrease in CAT function, as observed in our results. Moreover, the decrease observed in SOD activity could be due to a damage of enzymatic structure, function or enzymatic gene expression (Szymonik-Lesiuk et al., 2003). The liver is involved in numerous metabolic, immunological and endocrine functions with high blood vasculature. Despite the fenestration size depends on the animal species, it is known that sinusoidal fenestrae in C57BL/6 mice are 141 nm size (Jacobs et al., 2010),

565 which allows unrestricted passage of plasma components and nanohydrogels
566 (10–80 nm size range at physiological conditions) to the perisinusoidal space
567 ,where the cords of hepatocytes are situated (Bertrand and Leroux, 2012).
568 Inside the sinusoid capillaries, nanohydrogels could be phagocyted by the
569 Kupffer cells, via the recognition of opsonins on the nanohydrogels surface,
570 using fluid phase pinocytosis or endocytosis, due to their small size (Champion
571 et al., 2008; Petros and DeSimone, 2010). After ingestion, phagocytic vesicles
572 (phagosomes) coalesce with intracellular organelles containing digestive
573 proteins and an acidic internal pH, which may suppose a faster PTX release
574 from nanocarriers according to the cationic response of these nanohydrogels
575 (Perez et al., 2014) and the desintegration of the internalized polymeric
576 nanohydrogels. After desintegration, these nanosytems could be eliminated by
577 exocytosis or sequestered in residual bodies within the cell if it cannot be
578 digested (Bertrand and Leroux, 2012).
579
580 Besides, these drug delivery systems containing disulfide linkages such as N,
581 N'-cystaminebisacrylamide (CBA) can be reduced by glutathione molecule, as
582 *in vitro* studies demonstrated (Perez et al., 2014). In the present study, a
583 significant increase in GSSG-R activity was observed in spleen samples after
584 the treatment with PTX-loaded nanohydrogels (Fig. 6). Glutathione reductase
585 (GSSG-R) is involved in the maintenance of glutathione in reduced form (GSH)
586 by catalyzing the reduction of GSSG to GSH in the presence of NADPH (Zhang
587 and Kwong-Huat, 2000). As described above, the resulting GSH helps protect
588 cells from free radical damage by acting as an antioxidant non enzymatic agent.
589 In addition, an important part of the produced GSH content could disrupt

590 crosslinking agent (CBA) by reducing disulfide linkages of nanogel structure, as
591 observed in our previous *in vitro* studies (Perez et al., 2014). As
592 a consequence, glutathione reductase activity increases to maintain the
593 normal GSSG-GSH counterbalance.
594
595 Finally, kidney samples showed a significant increase of total
596 glutathione content (GSSG/GSH; Fig.6) in PTX-treated animals (free PTX and
597 PTX-loaded nanohydrogels). As other authors observed before (Mohamed
598 et al., 2014; Valko et al., 2006), oxidative stress response could induce an
599 increase of total glutathione content by increasing its synthesis. These
600 results could be explained by the kidneys function, as they are responsible
601 for blood filtration. This occurs through the glomerular capillary network of the
602 glomerulus, one of its components is the highly fenestrated endothelium. The
603 fenestration size (60 to 80 nm) makes difficult most of particulate drug delivery
604 systems to be filtered; consequently they could be retained (Bertrand and
605 Leroux, 2012) modifying the normal counterbalance of ROS production and, in
606 this way, the total glutathione content.

607 **5. Conclusions**

608 Nowadays, paclitaxel administration is associated with several side effects such
609 as hypersensitivity reactions, nephrotoxicity and neurotoxicity. In this study, we
610 have investigated the antitumor effect of PTX-loaded nanohydrogels to
611 overcome those side effects from conventional formulation. The results showed
612 that a single dose of PTX (30 mg/kg) when administered in NHA 80/15/5-
613 CBA stimuli-responsive nanohydrogels, led to significant enhancement of
614 tumor growth suppression and cellular apoptosis in sensitive HeLa
xenograft mice

615 model, with less toxicity than free PTX administration, as measured by changes
616 in blood biochemistry analysis. Based on these results, systemic administration
617 of PTX in biodegradable polymeric nanohydrogels delivery system could
618 be considered as a very effective strategy to be evaluated in further *in vivo*
619 assays in order to achieve the necessary therapeutic effect of PTX, and
620 overcome drug
621 resistance in cancer patients.

622 **6. Acknowledgements**

623 This work has been supported by MAT-2010-21509-C03-03 and UCM-
624 Banco Santander Research Groups Ref. GR3/14 (UCM-Group 920613).

625 **7. References**

626 Aebi, H. 1984. Catalase in vitro. Methods in Enzimology. 105, 121-126.
627
628
629 Agüero, L., Guerrero-Ramírez, L. and Katime, I. 2010. New Family of Functionalized
630 Monomers Based on Amines: A Novel Synthesis that Exploits the Nucleophilic
631 Substitution Reaction. Materials Sciences and Applications. 1, 103-108.
632
633 Andreopouloua, E. and Muggia, F. 2008. Pharmacodynamics of Tubulin and
634 Tubulin-Binding Agents: Extending Their Potential Beyond Taxanes. Clinical Breast
635 Cancer. 8, S54–S60.
636 Bertrand, N. and Leroux, J. C. 2012. The journey of a drug-carrier in the body: An
637 anatomo-physiological perspective. Journal of Controlled Release. 161, 152–163.
638
639 Blanco, M. D., Olmo, R. and Teijón, J. M. 2002. Hydrogels,New York.
640
641
642 Bradford, M. M. 1976. A rapid and sensitive method of the quantitation of
643 microgram quantities of protein utilizing the principle of protein-dye binding. Analytical
Biochemistry. 72, 248-254.
644
645 Crown, J. and O'Leary, M. 2000. The taxanes: an update. Lancet. 355, 1176-1178.
646
647 Champion, J. A., Walker, A. and Mitragotri, S. 2008. Role of particle size in
phagocytosis of polymeric microspheres. Pharmaceutical Research. 25, 1815–1821.

Chen, P., Cameron, R., Wang, J., Vallis, K. and Reilly, R. 2003. Antitumor Effects and Normal Tissue Toxicity of 111In-Labeled Epidermal Growth Factor Administered to Athymic Mice Bearing Epidermal Growth Factor Receptor–Positive Human Breast Cancer Xenografts. J. Nuclear Medicine. 44, 1469-1478.

Chun, C., Lee, S. M., Kim, S. Y., Yang, H. K. and Song, S. C. 2009. Thermosensitive poly(organophosphazene)-paclitaxel conjugate gels for antitumor applications. Biomaterials. 30, 2349-2360.

Engin, K., Leeper, D. B., Cater, J. R., Thistlethwaite, A. J., Tupchong, L. and Mcfarlane, J. D. 1995. Extracellular Ph Distribution in Human Tumors. International Journal of Hyperthermia. 11, 211-216.

Fleige, E., Quadir, M. A. and Haag, R. 2012. Stimuli-responsive polymeric nanocarriers for the controlled transport of active compounds: Concepts and applications. Advanced Drug Delivery Reviews. 64, 866-884.

Gao, Z. G., Lee, D. H., Kim, D. I. and Bae, Y. H. 2005. Doxorubicin loaded pH-sensitive micelle targeting acidic extracellular pH of human ovarian A2780 tumor in mice. Journal of Drug Targeting. 13, 391-397.

Goodman, C. M., McCusker, C. D., Yilmaz, T. and Rotello, V. M. 2004. Toxicity of gold nanoparticles functionalized with cationic and anionic side chains. Bioconjugate Chemistry. 15, 897-900.

Gupta, P., Vermani, K. and Garg, S. 2002. Hydrogels: from controlled release to pH-responsive drug delivery. Drug Discovery Today. 7, 569–579.

Hull, L. C., Farrell, D. and Grodzinski, P. 2014. Highlights of recent developments and trends in cancer nanotechnology research-View from NCI Alliance for Nanotechnology in Cancer. Biotechnology Advances. 32, 666-678.

Humason, G. L., Ed. (1979). Animal Tissue Techniques. New York, W.H. Freeman.

Iqbal, J., Sarti, F., Perera, G. and Bernkop-Schnürch, A. 2011. Development and in vivo evaluation of an oral drug delivery system for paclitaxel. Biomaterials. 32, 170-175.

Jacobs, F., Wisse, E. and De Geest, B. 2010. The Role of Liver Sinusoidal Cells in Hepatocyte-Directed Gene Transfer. The American Journal of Pathology. 176, 14-21.

Jemal, A., Bray, F., Center, M., Ferlay, J., Ward, E. and Forman, D. 2011. Global Cancer Statistics. Cancer Journal for Clinicians. 61, 69–90.

Kalaria, D. R., Sharma, G., Beniwal, V. and Ravi, M. N. V. 2009. Design of Biodegradable Nanoparticles for Oral Delivery of Doxorubicin: In vivo Pharmacokinetics and Toxicity Studies in Rats. Pharmaceutical Research. 26,

Kim, S., Wook, D., Ho, Y., Seok, J., Seung, H., Wan, S. and Hyo, M. 2001. In vivo evaluation of polymeric micellar paclitaxel formulation: toxicity and efficacy. Journal of Controlled Release. 72, 191-202.

Klinger, D. and Landfester, K. 2012. Stimuli-responsive microgels for the loading and release of functional compounds: Fundamental concepts and applications. Polymer. 53, 5209-5231.

Kumar, A., Hoskins, P. J. and Tinker, A. V. 2015. Dose-dense Paclitaxel in Advanced Ovarian Cancer. Clinical Oncology. 27, 40-47.

Kuppusamy, P., Afeworki, M., Shankar, R. A., Coffin, D., Krishna, M. C., Hahn, S., Mitchell, J. B. and Zweier, J. L. 1998. In vivo electron paramagnetic resonance imaging of tumor heterogeneity and oxygenation in a murine model. Cancer Research. 58, 1562-1568.

Kwon, J., Drumright, R., Siegwart, D. and Matyjaszewski, K. 2008. The development of microgels/nanogels for drug delivery applications. Progress in Polymer Science. 33, 448-477.

Lee, E. S., Gao, Z. G. and Bae, Y. H. 2008. Recent progress in tumor pH targeting nanotechnology. Journal of Controlled Release. 132, 164-170.

Li, F., Wu, H., Zhang, H., Li, F., Gu, C. H. and Yang, Q. 2009. Antitumor drug Paclitaxel-loaded pH-sensitive nanoparticles targeting tumor extracellular pH. Carbohydrate Polymers. 77, 773-778.

Li, S. D. and Huang, L. 2008. Pharmacokinetics and biodistribution of nanoparticles. Mol.Pharmacol. 5, 496-504.

Lia, F., Wua, H., Zhanga, H., Fei Lia, Gub, C. and Yang, Q. 2009. Antitumor drug Paclitaxel-loaded pH-sensitive nanoparticles targeting tumor extracellular pH. Carbohydrate Polymers. 77, 773–778.

Liu, Z., Chen, K., Davis, C., Sherlock, S., Cao, Q., Chen, X. and Dai, H. 2008. Drug Delivery with Carbon Nanotubes for In vivo Cancer Treatment. Cancer Research. 68, 6652-6660.

Mayer, A., Vadon, M., Rinner, B., A. Novak, A., Wintersteiger, R. and Frohlich, E. 2009. The role of nanoparticle size in hemocompatibility. Toxicology. 258, 139-147.

732 Meng, F., Hennink, W. E. and Zhong, Z. 2009. Reduction-sensitive polymers and bioconjugates
733 for biomedical applications. Biomaterials. 30, 2180-2198.

734
735 Mo-ying, P., Xiu-xiong, N., Y., Q. and Hong, Z. H. 2004. A comparative study on the
736 liver injuries induced by Paclitaxel and Cyclophosphamide. Medicine and Pharmacy. 3,
0-10.
737
738
739 Moghimi, S. M., Hunter, A. C. and Murray, J. C. 2001. Long-circulating and
target-specific nanoparticles: theory to practice. Pharmacol Rev. 52, 283-318.
740
741
742 Mohamed, M., Mohammad, M., Zakaria, A., Ghazali, N., Isa, M., Razak, H. and Saad,
743 W. 2014. Induction of Oxidative Stress Following Low Dose Ionizing Radiation in ICR
Mice. World Journal of Medical Sciences 10, 198-203.
744
745
746 Motornov, M., Roiter, Y., Tokarev, I. and Minko, S. 2010. Stimuli-responsive
747 nanoparticles, nanogels and capsules for integrated multifunctional intelligent
systems. Progress in Polymer Science. 35, 174-211.
748
749
750 Oberdörster, G., Oberdörster, E. and Oberdörster, J. 2005. Nanotoxicology: an
751 emerging discipline evolving from studies of ultrafine particles. Environmental Health
Perspectives. 113, 823-839.
752
753
754 Pagel, J., Hedin, N., Subbiah, K., Meyer, D., Mallet, R., Axworthy, D., Theodore, L.,
755 Scott , D., Matthews, D. and Press, O. 2003. Comparison of anti-CD20 and anti-
756 CD45 antibodies for conventional and pretargeted radioimmunotherapy of B-cell
lymphomas. Blood. 101, 2340-2348.
757
758
759 Panchagnula, R. 1998. Pharmaceutical aspects of paclitaxel. International
Journal of Pharmaceutics. 172, 1-15.
760
761
762 Patel, V. R. and Amiji, M. M. 1996. Preparation and characterization of freeze-dried
763 chitosan-poly(ethylene oxide) hydrogels for site-specific antibiotic delivery in
the stomach. Pharmaceutical Research. 13, 588-593.
764
765
766 Peppas, N. A., Bures, P., Leobandung, W. and Ichikawa, H. 2000. Hydrogels in
pharmaceutical formulations. European Journal of Pharmaceutics and
767 Biopharmaceutics. 50, 27-46.
768
769
770 Perez, E., Fernandez, A., Olmo, R., Teijon, J. M. and Blanco, M. D. 2014. pH and
glutathion-responsive hydrogel for localized delivery of paclitaxel. Colloids and
771 Surfaces B-Biointerfaces. 116, 247-256.
772
773

Petros, R. A. and DeSimone, J. M. 2010. Strategies in the design of
nanoparticles for therapeutic applications. Nature Reviews Drug Discovery. 9,
615-627.

Qiao, Z. Y., Zhang, R., Du, F. S., Liang, D. H. and Li, Z. C. 2011. Multi-responsive nanogels containing motifs of ortho ester, oligo(ethylene glycol) and disulfide linkage as carriers of hydrophobic anticancer drugs. Journal of Controlled Release. 152, 57-66.

Qiu, Y. and Park, K. 2012. Environment-sensitive hydrogels for drug delivery. Advanced Drug Delivery Reviews. 64, 49–60.

Reul, R., Renette, T., Bege, N. and Kissel, T. 2011. Nanoparticles for paclitaxel delivery: A comparative study of different types of dendritic polyesters and their degradation behavior. International Journal of Pharmaceutics. 407, 190–196.

Riva, G., Baronchellia, S., Paolettaa, L., Buttaa, V., Biunnob, I., Lavitranoa, M., Dalpràa, L. and Bentivegna, A. 2014. In vitro anticancer drug test: A new method emerges from the model of glioma stem cells. Toxicology Reports. 1, 188–199.

Sharifi, S., Bhezadi, S., Laurent, M., Forrest, S., Stroeve, P. and Mahmoudi, M. 2012. Toxicity of nanomaterials. Chemistry Society Review. 41, 2323-2343.

Shim, W., Kim, J.-H., Kim, K., Kim, Y.-S., Park, R.-W., Kim, I.-S., Kwon, I. and Lee, D. 2007. pH- and temperature-sensitive, injectable, biodegradable block copolymer hydrogels as carriers for paclitaxel. International Journal of Pharmaceutics. 331, 11–18.

Simmons, K. 1984. Defense against free radicals has therapeutic implications. JAMA. 251, 2187–2192.

Singla, A. K., Garg, A. and Aggarwal, D. 2002. Paclitaxel and its formulations. International Journal of Pharmaceutics. 235, 179-192.

Song, N., Liu, W., Tu, Q., Liu, R., Zhang, Y. and Wang, J. 2011. Preparation and in vitro properties of redox-responsive polymeric nanoparticles for paclitaxel delivery. Colloids Surface B Biointerfaces. 87, 454-463.

Spencer, C. M. and Faulds, D. 1994. Paclitaxel: a review of its pharmacodynamic and pharmacokinetic properties and therapeutic potential in the treatment of cancer. Drugs. 48, 794–847.

Steichen, S., Caldorera-Moore, M. and Peppas, N. 2013. A review of current nanoparticle and targeting moieties for the delivery of cancer therapeutics. Eur J Pharm Sci. 48, 416-427.

Szymonik-Lesiuk, S., Czechowska, G., Stryjecka-Zimmer, M., Siomka, M., Madro, A., Celinski, K. and Wielosz, M. 2003. Catalase, superoxide dismutase, and glutathione peroxidase activities in

various rat tissues after carbon tetrachloride intoxication. Journal Hepatobiliary Pancreatic Science. 10, 309-315.

Tannock, I. F. and Rotin, D. 1989. Acid Ph in Tumors and Its Potential for Therapeutic Exploitation. Cancer Research. 49, 4373-4384.

Tozuka, K., Horiguchi, J., Takata, D., Rokutanda, N., Nagaoka, R., Tokiniwa, H., Kikuchi, M., Satou, A., Takei, H. and Takeyosh, I. 2013. Collagen gel droplet-embedded culture-drug sensitivity test and Ki67 expression in estrogen receptor-positive and HER2-negative breast cancer. Molecular Clinical Oncology. 1, 93-99.

Valko, M., Rhodes, C. J., Moncol, J., Izakovic, M. and Mazur, M. 2006. Free radicals, metals and antioxidants in oxidative stress-induced cancer. Chemico-Biological Interactions. 160, 1-40.

Wang, F., Shen, Y., Xu, X., Lv, L., Yanggong Li, Liu, J., Li, M., Guo, A., Guo, S. and Jin, F. 2013. Selective tissue distribution and long circulation endowed by paclitaxel loaded PEGylated poly(e-caprolactone-co-L-lactide) micelles leading to improved anti-tumor effects and low systematic toxicity International Journal of Pharmaceutics 456, 101- 112

Yared, J. A. and Tkaczuk, K. H. R. 2012. Update on taxane development: new analogs and new formulations. Drug Design Development and Therapy. 6, 371-384.

Zhang, C., Qu, G., Sun, Y., Wu, X., Yao, Z., Guo, Q., Ding, Q., Yuan, S., Shen, Z., Ping, Q. and Zhou, H. 2008. Pharmacokinetics, biodistribution, efficacy and safety of N-octyl-O-sulfate chitosan micelles loaded with paclitaxel. Biomaterials. 29, 1233-1241.

Zhang, X. F. and Kwong-Huat, B. 2000. Antihyperglycaemic and anti-oxidant properties of Andrographis paniculata in normal and diabetic rats. Clinical and Experimental Pharmacology and Physiology. 27, 358–363.

Zhang, Y., Chan, H. and Leong, K. 2013. Advanced materials and processing for drug delivery: The past and the future. Advanced Drug Delivery Reviews. 65, 104–120.

Table 1

Treatments	T(days)	Tumor growth rates (r^2)	Tumor growth ratio
Control	14-30 30-39	21.9 (0.912) 94.5 (0.989)	V_2/V_1= 1.7 V_3/V_1= 7.3
Unloaded NHA 80/15/5-CBA	14-30 30-39	42.6 (0.969) 58.5 (0.959)	V_2/V_1= 3.3 V_3/V_1= 4.5
Free PTX	14-30 30-39	33.0 (0.985) 36.9 (0.947)	V_2/V_1= 2.6 V_3/V_1= 2.9
PTX-NHA 80/15/5-CBA	14-30 30-39	20.6 (0.900) 8.01 (0.956)	V_2/V_1= 1.6 V_3/V_1= 0.6

V_1 represents tumor growth rate before PTX treatment; V_1 = 12.9 mm^3/day.
V_2 represents tumor growth rate among the day 14 to 30.
V_3 represents tumor growth rate among the day 30 to 39.

Table 1. Tumor growth rate (mm^3/day) and tumor growth ratio. T (days) indicates the time, in days, considered in each analyzed phase. Two different stages were observed (stage I: from day 14 to day 30; stage II: from day 30 to day 39) along the tumor evolution experiment period.

Table 2

Treatment	AST (U/L)	ALT (U/L)	ALP (U/L)	BUN (mg/dL)	CRE (µmol/L)
Control	244.5 ± 48.8	31.7 ± 2.4	113.0 ± 33.7	18.7 ± 0.2	53.4 ± 2.6
Free PTX	294.9 ± 31.1	84.4 ± 7.9*+	168.8 ± 31.0	21.5 ± 2.8	27.1 ± 2.6*+
Unloaded NHA 80/15/5- CBA	178.3 ± 44.7	23,3 ± 4.7	154.7 ± 58.4	19.2 ± 3.3	47.9 ± 2.3
PTX-NHA 80/15/5-CBA	157.2 ± 21.2	39.7 ± 13.3	160.5 ± 40.1	18.7 ± 2.8	36.9 ± 3.5

All data are the mean ± SD (n=6).

* $P < 0.05$ when compared with the normal saline (control group).

+ $P < 0.05$ when compared with PTX-NHA 80/15/5-CBA.

Table 2. Biochemical blood analysis of female athymic nude mice bearing HeLa human tumor xenografts after treatments: untreated (control) and treated with unloaded-NHA 80/15/5 CBA, PTX-NHA 80/15/5-CBA and free PTX at the dose of 30mg/kg. AST: aspartate aminotransferase; ALT: alanine aminotransferase; ALP: alkaline phosphatase; BUN: blood urea nitrogen and CRE: creatinine.

Figure 1

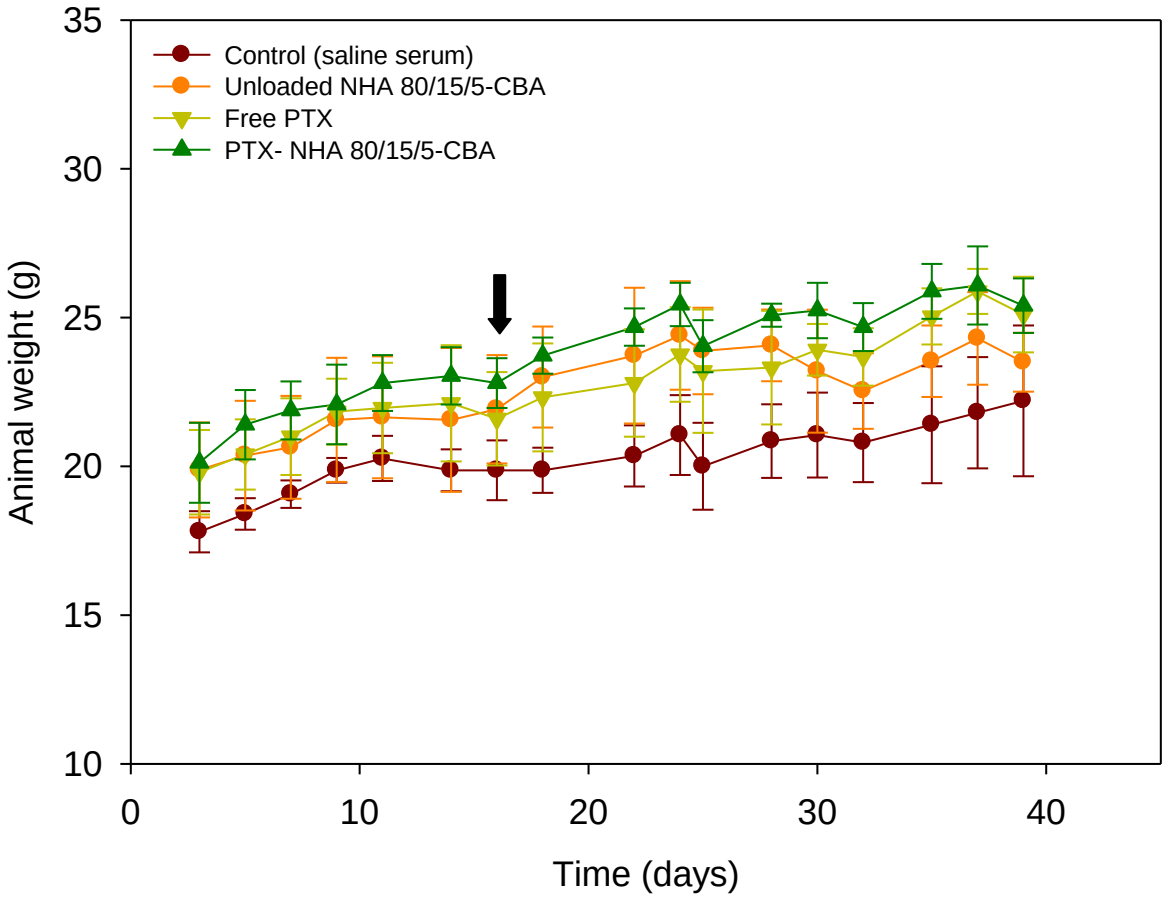

Figure 1. Mean body weight change in female athymic nude mice bearing HeLa human tumor xenografts treated with either saline, unloaded nanohydrogels, PTX-loaded nanohydrogels or PTX at a dose of 30 mg/kg subcutaneously injected (dark arrow). Each point represents mean ± SD (n=6).

Figure 2

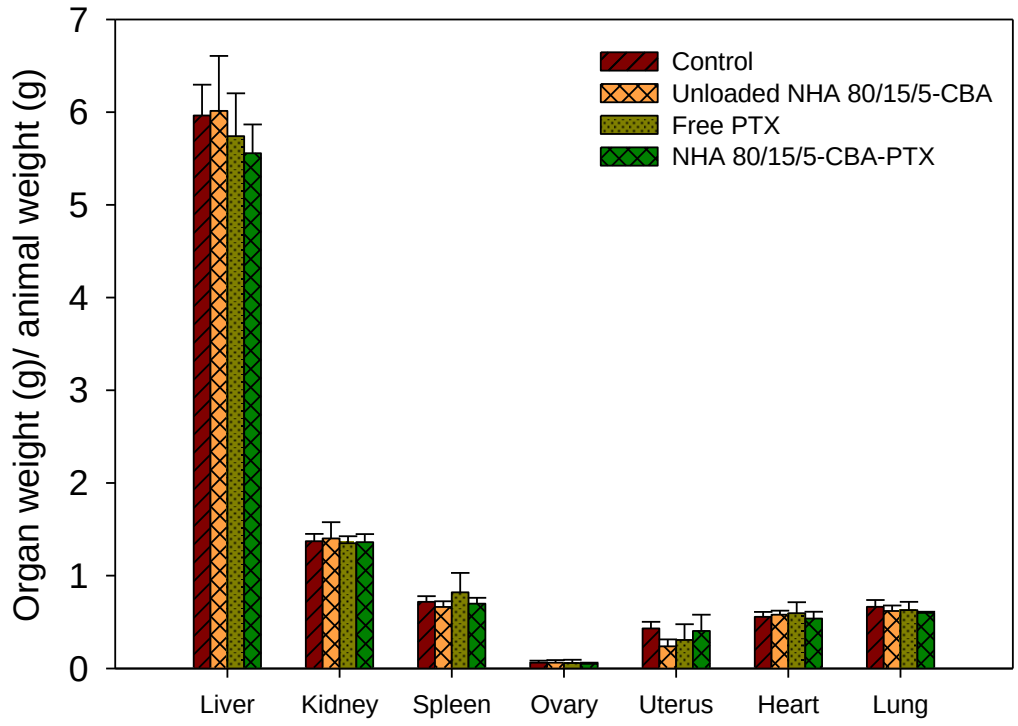

Figure 2: Organosomatic index of the organs extracted from female athymic nude mice bearing HeLa human tumor xenografts after the different treatments. All data are the mean ± SD (n=6).

Figure 3

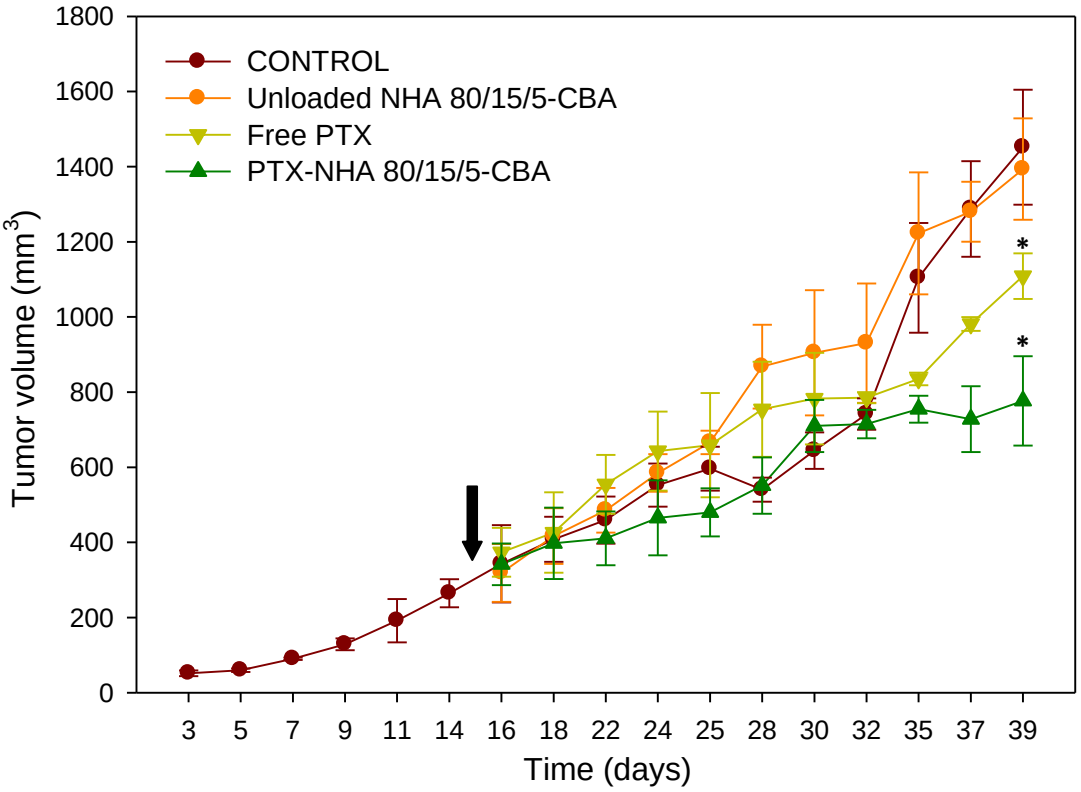

* $p < 0.01$ when compared with the normal saline.

Figure 3. Antitumor effect of unloaded nanohydrogels (NHA 80/15/5-CBA), PTX-loaded nanohydrogels (PTX-NHA 80/15/5-CBA) and free PTX in female athymic nude mice bearing HeLa human tumor xenografts. Two weeks after subcutaneous HeLa injection, treatments were injected subcutaneously in a single dose (black arrow). Untreated control received saline serum injection; the treatments groups consisted in unloaded nanohydrogels, PTX-loaded nanoparticles and free PTX (considering PTX concentration 30 mg/kg). All data are the mean ± SD (n=6).

Figure 4

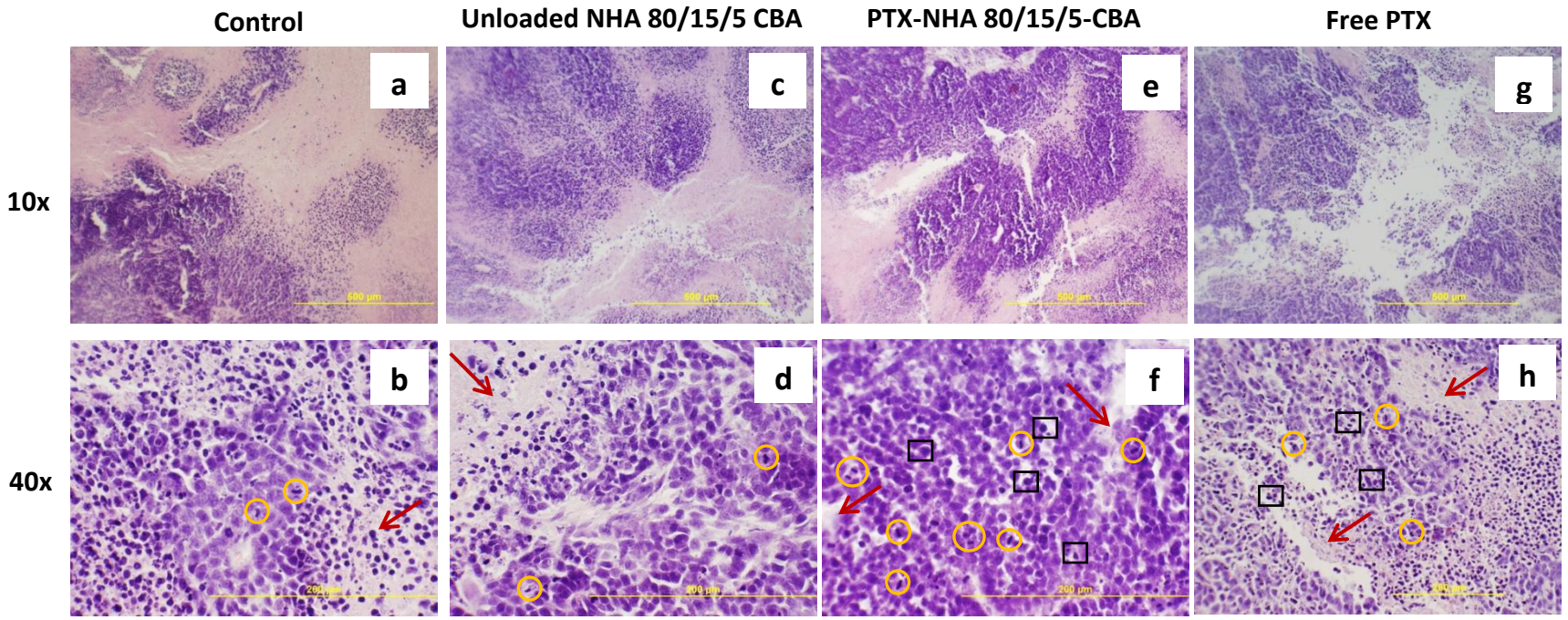

Figure 4. Histological appearance of the epithelial-like cortex of HeLa cell untreated tumor (a-b), unloaded NHA 80/15/5-CBA nanohydrogels treated tumor (c-d); PTX-loaded NHA 80/15/5-CBA nanohydrogels treated tumor (e-f) and free PTX treated tumor (g-h), using the hematoxylin-eosin staining method (magnifications 10x and 40x). Yellow circles indicate the presence of cells in different stages of mitotic division. Arrows indicate the presence of necrosis areas and squares show the presence of apoptotic bodies. Yellow bars represent 200 µm.

Figure 5

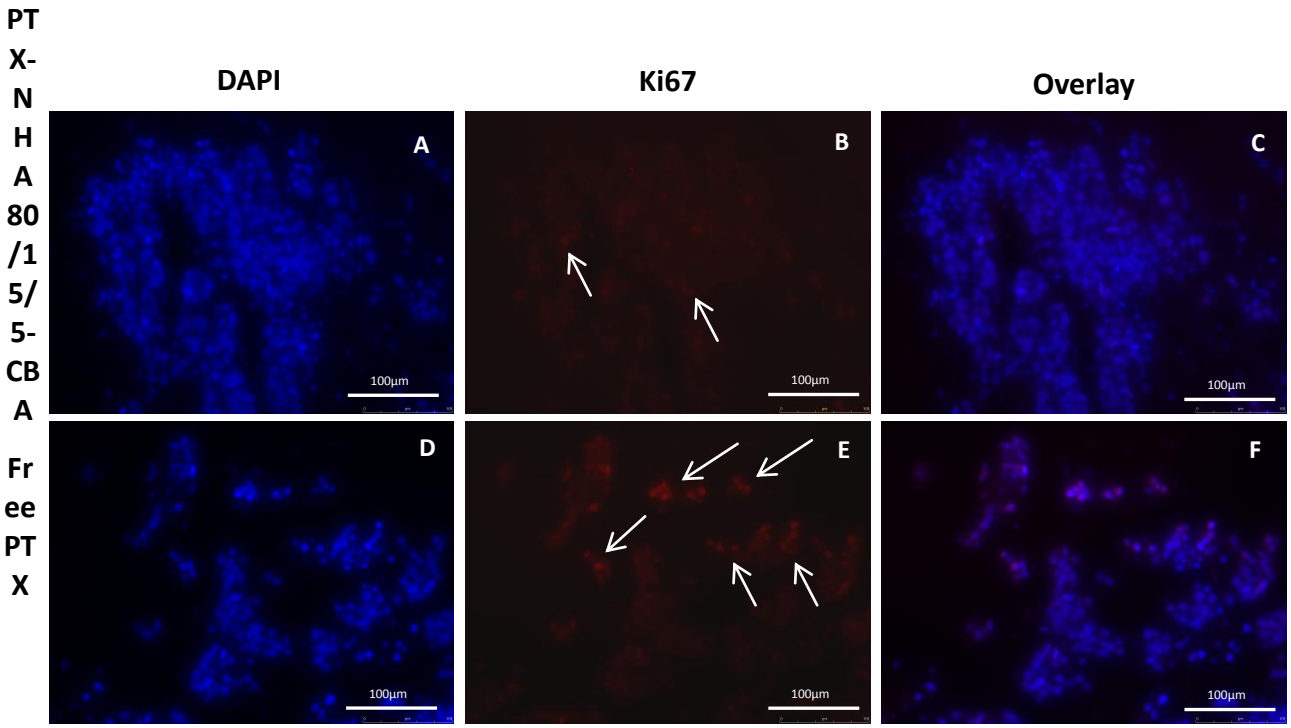

Figure 5. Representative images of the immunohistochemical detection of Ki-67 antigen (proliferation assay) in HeLa xenograft tumor samples using the fluorescent method: PTX-loaded nanohydrogel treated tumor (A-C) and free PTX treated tumor tissues (D-F). In blue is represented the nuclear staining with DAPI. In red, the nuclear fluorescent signal due to the presence of Ki-67 proliferating antigen. Overlay indicates the visualization of both co-staining images. Arrows indicate the presence of some Ki-67 positive nuclei in tumor tissues. White bars represent 100µm.

Figure 6

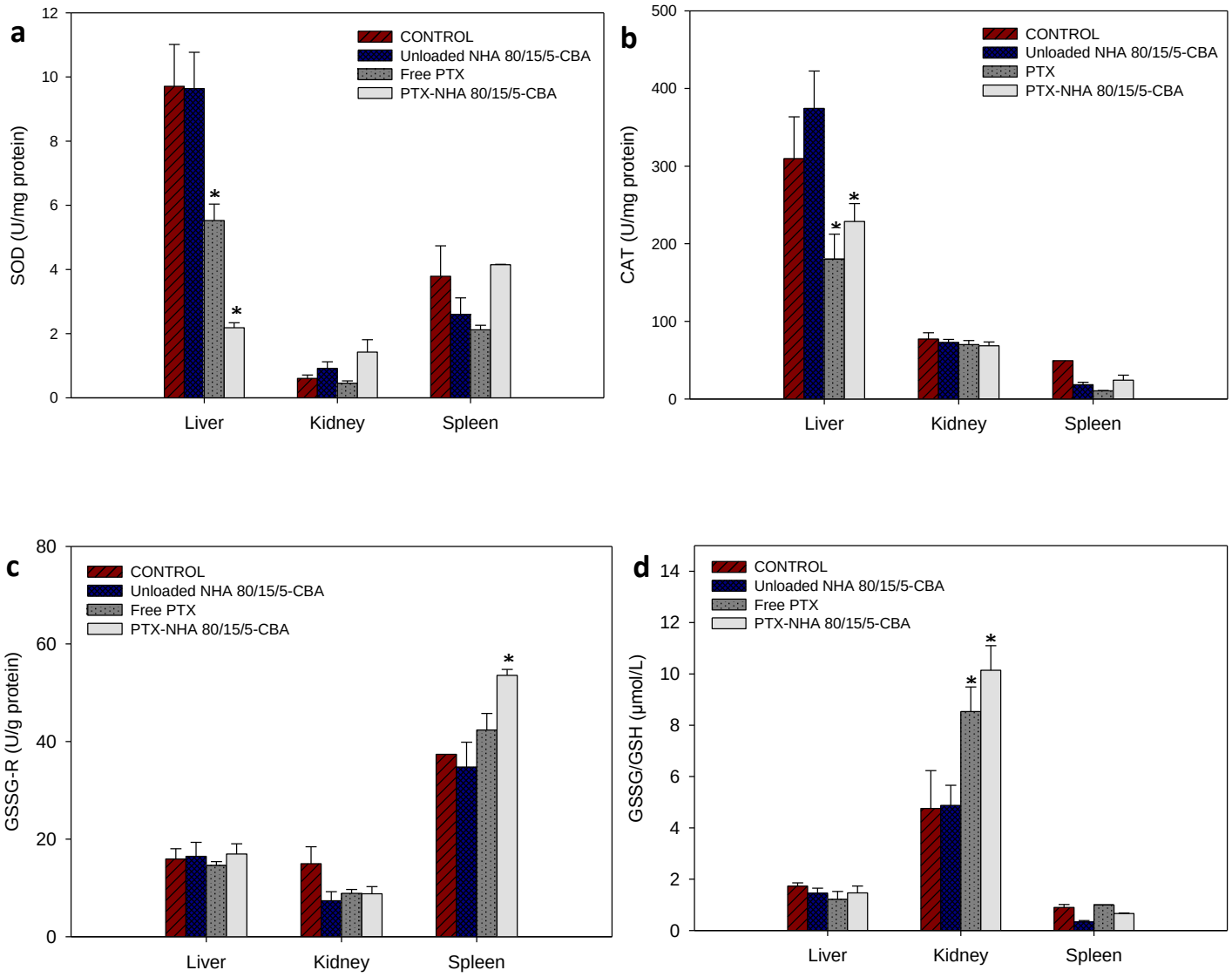

All data are the mean ± SD (n=6). * $p < 0.05$ when compared with the normal saline (control group).

Figure 6: Antioxidant determinations from liver, kidney and spleen of female athymic nude mice bearing HeLa human tumor xenografts after treatments. (a) superoxide dismutase activity (SOD); (b) catalase activity (CAT); (c) glutathione reductase activity (GSSG-R) and (d) total glutathione content (GSSG/ GSH).

Supplementary Material

Click here to download Supplementary Material: Fig. A.1. Histology tumor images.docx

Supplementary Material

Click here to download Supplementary Material: Fig. A.2. Immunohistochemical images.docx

Supplementary Material A.1

Click here to download Supplementary Material: Fig. A.1. Inmunohistochemical images.docx

Supplementary Material A.2

Click here to download Supplementary Material: Fig. A.2. Histology tumor images.docx

Highlights

- PTX-loaded NG enhanced tumor growth suppression in Hela xenograft models.
- PTX-NG treated tumors showed apoptotic bodies and several mitotic figures.
- PTX-NG treated tumors revealed a lower presence of Ki 67 proliferation marker.
- Biochemical data showed no kidney or liver damage after PTX-NG injection.
- PTX (30 mg/kg) modified antioxidant defenses in liver, kidney and spleen.

Figure 5

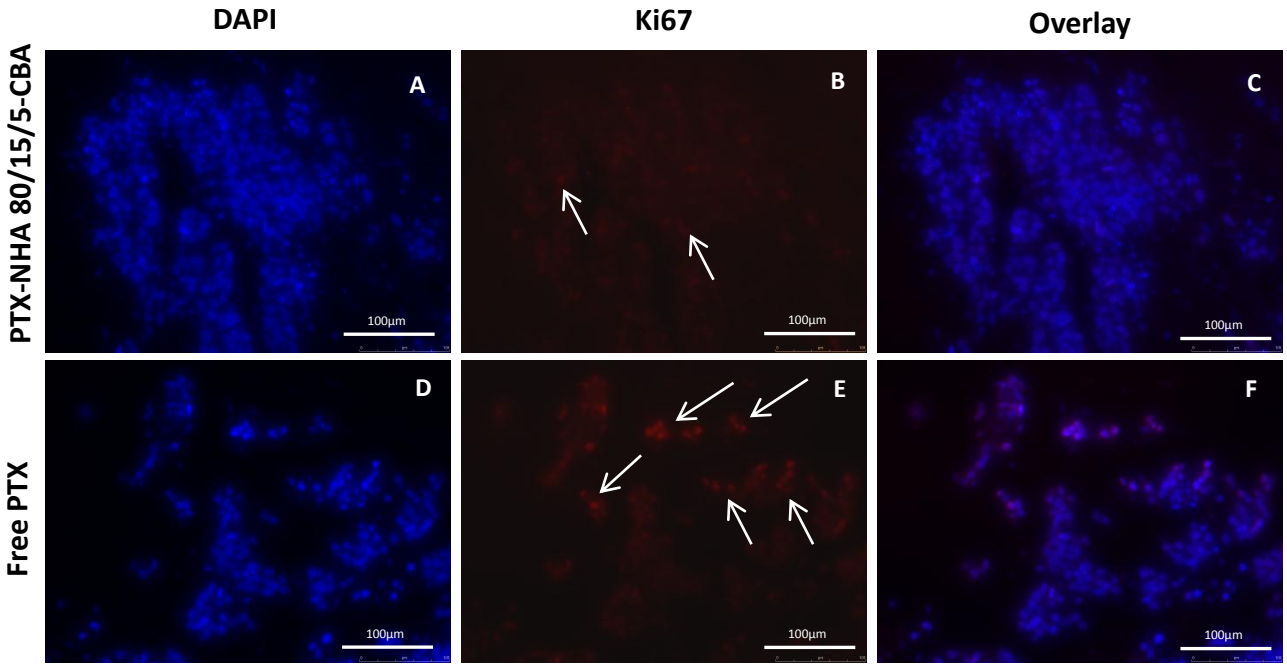

Figure 5. Representative images of the immunohistochemical detection of Ki-67 antigen (proliferation assay) in HeLa xenograft tumor samples using the fluorescent method: PTX-loaded nanohydrogel treated tumor (A-C) and free PTX treated tumor tissues (D-F). In blue is represented the nuclear staining with DAPI. In red, the nuclear fluorescent signal due to the presence of Ki-67 proliferating antigen. Overlay indicates the visualization of both co-staining images. Arrows indicate the presence of some Ki-67 positive nuclei in tumor tissues. White bars represent 100µm.